Human BRCA1–BARD1 ubiquitin ligase activity counteracts chromatin barriers to DNA resection

Ruth M Densham[1], Alexander J Garvin[1], Helen R Stone[1], Joanna Strachan[1,5], Robert A Baldock[2], Manuel Daza-Martin[1], Alice Fletcher[1], Sarah Blair-Reid[1], James Beesley[1], Balraj Johal[1], Laurence H Pearl[2], Robert Neely[3], Nicholas H Keep[4], Felicity Z Watts[2] & Joanna R Morris[1]

[1]Birmingham Centre for Genome Biology, Institute of Cancer and Genomic Sciences, University of Birmingham, Birmingham, UK.
[2]Genome Damage and Stability Centre, School of Life Sciences, University of Sussex, Brighton, UK.
[3]School of Chemistry, University of Birmingham, Birmingham, UK.
[4]Department of Biological Sciences, Institute for Structural and Molecular Biology, Birkbeck, University of London, London, UK.
[5]Present address: Institute of Cell Biology, University of Edinburgh, Edinburgh, UK.
Correspondence should be addressed to J.R.M. (j.morris.3@bham.ac.uk).

Abstract

The opposing activities of 53BP1 and BRCA1 influence pathway choice in DNA double-strand-break repair. How BRCA1 counteracts the inhibitory effect of 53BP1 on DNA resection and homologous recombination is unknown. Here we identify the site of BRCA1–BARD1 required for priming ubiquitin transfer from E2~ubiquitin and demonstrate that BRCA1–BARD1's ubiquitin ligase activity is required for repositioning 53BP1 on damaged chromatin. We confirm H2A ubiquitination by BRCA1–BARD1 and show that an H2A-ubiquitin fusion protein promotes DNA resection and repair in BARD1-deficient cells. BRCA1–BARD1's function in homologous recombination requires the chromatin remodeler SMARCAD1. SMARCAD1 binding to H2A-ubiquitin and optimal localization to sites of damage and activity in DNA repair requires its ubiquitin-binding CUE domains. SMARCAD1 is required for 53BP1 repositioning, and the need for SMARCAD1 in olaparib or camptothecin resistance is alleviated by 53BP1 loss. Thus, BRCA1–BARD1 ligase activity and subsequent SMARCAD1-dependent chromatin remodeling are critical regulators of DNA repair.

Inheritance of a mutation in breast cancer susceptibility gene 1 (*BRCA1*) confers a high risk of breast and ovarian cancer, and tumors in carriers of *BRCA1* gene mutations are characterized by excessive genome instability. The BRCA1 protein has been implicated in several aspects of genome stability including checkpoint promotion, DNA cross-link repair, replication-fork stability and DNA double-strand break (DSB) repair[1–3]. In DSB repair, BRCA1 is most prominently associated with homologous recombination (HR), in which it promotes the essential step of DNA resection by opposing the block on resection contributed by the p53-binding protein 53BP1 and its effector proteins (reviewed in refs. 3,4). In the absence of BRCA1, DSBs are repaired by toxic nonhomologous end joining (NHEJ)[5]. BRCA1 associates with the resection protein CtIP and subsequently relieves the 53BP1 block[6], but how BRCA1 contributes to this process is not known.

In people with familial breast and ovarian cancer, pathogenic and unclassified substitution variants in the *BRCA1* gene have been found across the region encoding the first 100 amino acids (aa). This part of BRCA1 contacts its heterodimeric binding partner, the BRCA1-associated RING-domain protein, BARD1, and E2 ubiquitin (Ub)-conjugating enzymes, thereby allowing BRCA1–BARD1 to function as an E3 Ub ligase in the transfer of Ub from E2-conjugating enzymes to target proteins[7]. Several targets have been proposed, and recently BRCA1-mediated ubiquitination of histone H2A has been mapped[8]. However the role, if any, of the BRCA1 E3 Ub ligase activity in DNA repair has been controversial [9–11]. Evidence from *Brca1*-deficient mice has suggested that H2A ubiquitination regulates global heterochromatin integrity and, through transcriptional repression of satellite RNA, is responsible for multiple disparate cellular functions of Brca1, including the promotion of genomic integrity[9]. How increased satellite RNA affects HR repair is not clear, and the phenomenon of increased satellite RNA expression has not been universally observed in *Brca1*-deficient models[12]. Indeed, other models of Brca1 dysfunction have suggested a restricted role, or no role, for its biochemical function in DNA repair[10,11].

Here, we sought to investigate the role of the BRCA1–BARD1 Ub ligase activity in the DNA-damage response in human cells. Our data suggest a model in which chromatin modification by BRCA1–BARD1 E3 Ub ligase activity repositions 53BP1 and drives completion of resection through promoting the activity of the SWI/SNF-related matrix-associated actin-dependent regulator of chromatin (SMARCAD1).

RESULTS

A charged residue required in type 1 RING–RING E3s

Ub-priming structures that promote the transfer of the donor Ub from a Ub-loaded E2 conjugating enzyme have been identified in RING finger protein 4 (RNF4) and Casitas B-lineage lymphoma (C-CBL) E3 Ub ligases [13,14]. However, no analogous surfaces have been found in E3 Ub ligases characterized by helical interactions between protomers, known as type 1 ligases (ref. 15); these include the human homolog of yeast radiation mutant 18 (RAD18), the Polycomb-repressor-complex ligase RING1A or RING1B complexes and BRCA1–BARD1. Nevertheless minimal BRCA1–BARD1 N-terminal fragments exhibit base-level Ub ligase activity [16,17], thus indicating that the elements necessary for Ub transfer are present within the polypeptides.

To identify a possible Ub-binding interface, we overlaid the RNF4–RNF4–Ub~E2 structure (PDB 4AP4 (ref. 13)) onto N-terminal BRCA1–BARD1 (PDB 1JM7 (ref. 18)). In the superposition, BARD1 residues 91–99 are in a similar location to the RNF4 residue Y193, which engages Ub13. A mutational scan across the BARD1 region revealed that a heterodimer bearing a substitution at R99 exhibited decreased activity (**Supplementary Fig. 1a**,**b**). Substitution of R99 to a lysine was tolerated, but the activity of the heterodimer with glutamate (R99E) was severely impaired for all Ub-conjugating enzymes of the Ub-conjugating enzyme 2D (UBE2D) family (**Fig. 1a** and **Supplementary Fig. 1c**–**e**). Substitutions at R99 did not affect BARD1's interaction with BRCA1 (**Fig. 1b**), but the R99E-mutant heterodimer showed a weaker interaction with conjugation-proficient E2 (**Supplementary Fig. 1f**).

In the superimposition, R99 of BARD1 is predicted to be close to the D32 side chain of Ub (**Supplementary Fig. 1g**). To test whether R99 of BARD1 contacts Ub, we generated a D32R mutation in Ub. This mutant, compared with wild-type (WT) Ub, was processed slightly less well by the BRCA1–BARD1 heterodimer, but the weak catalytic activity of the R99E BARD1-mutant heterodimer substantially improved with D32R Ub (**Fig. 1c**), thus suggesting contact with Ub contributes to activity. Transfer reactions of Ub from UBE2D1 or UBE2D3 E2 enzymes to free lysine revealed decreased discharge rates with the R99E heterodimer than with WT proteins (**Fig. 1d** and **Supplementary Fig. 1h**). Thus, R99 of BARD1 promotes heterodimer interaction with the Ub~E2 thioester conjugate through Ub and is required to promote the discharge of Ub from the E2 contacting BRCA1.

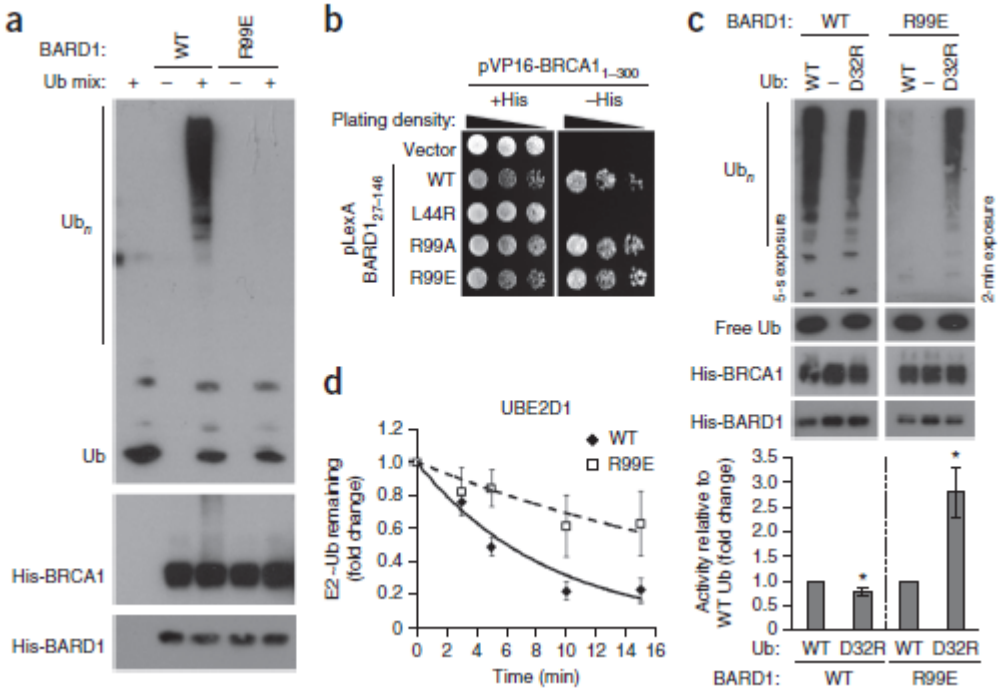

Figure 1 A basic residue of BARD1 promotes Ub transfer from BRCA1–E2~Ub. ***(a)*** *Western blots probed for BRCA1, His_6 (BARD1) and Ub, comparing the ability of the BRCA1–BARD1 heterodimer containing WT BARD1 or R99E BARD1 to catalyze the formation of Ub chains. Ub mix refers to E1, E2, Ub, ATP and ligase reaction buffer.* ***(b)*** *Yeast two-hybrid assays showing that the BRCA1–BARD1 heterodimer is not disrupted by BARD1 R99 variants. Yeast strains expressed VP16 $BRCA1_{1–300}$ with WT and substituted LexA-$BARD1_{27–146}$ (100 mM 3-amino-1,2,4-triazole (3-AT)). L44R is included as a heterodimer-disruptive control*[19]*.* ***(c)*** *Western blots showing improved activity of the R99E BARD1 heterodimer with D32R mutant Ub. Graph shows quantification (mean ± s.e.m.) of high-molecular-weight Ub from four independent experiments. (The R99E-heterodimer reaction was exposed longer than the control.) *P < 0.05 by two-sided Student's t test.* ***(d)*** *In vitro assays showing the ability of WT and R99E BARD1 heterodimers to discharge Ub from a loaded E2~Ub dimer. Results show mean ± s.e.m. from four independent experiments. Uncropped blot images are shown in* ***Supplementary Data Set 1****; Source Data for graphs can be found online.*

We noted that other type 1 RING E3 ligases carry positively charged residues (arginine or lysine) at positions analogous to R99 of BARD1 (**Fig. 2a** and **Supplementary Fig. 2a**). For example, in the heterodimeric complex of B cell-specific Moloney murine leukemia virus integration site 1 (BMI1; also known as Polycomb-group RING-finger protein 4 (PCGF4)) with RING1B, the 'inactive' partner, BMI1, has an equivalent lysine, K73, whereas the protomer contacting the E2, RING1B, lacks a similarly located charged residue (as does BRCA1). We mutated K73E in BMI1 and R76A in RAD18. Whereas ectopically expressed WT RAD18 induced PCNA monoubiquitination and also potentiated PCNA monoubiquitination after UV exposure, the R76A mutant did not (**Fig. 2b**). Similarly, the K73E BMI1–RING1B heterodimer was unable to catalyze monoubiquitination of H2A in nucleosomes *in vitro* (**Fig. 2c**; copurification in **Supplementary Fig. 2b**). In cells, ectopic expression of K73E BMI1 but not WT protein inhibited DSB Ub signaling, and WT BMI1 but not K73E BMI1 rescued repair of a gene-conversion substrate in cells depleted of endogenous BMI1 (**Supplementary Fig. 2c–e**). These

data are consistent with the effects of inhibition of RING1A and RING1B19. We suggest that a charged interface between type 1 dimeric RING E3 ligases and the donor Ub activates the E2~Ub thioester. In the two heterodimeric complexes, this key interface is provided by protomers previously described as simply scaffold proteins, BARD1 and BMI1.

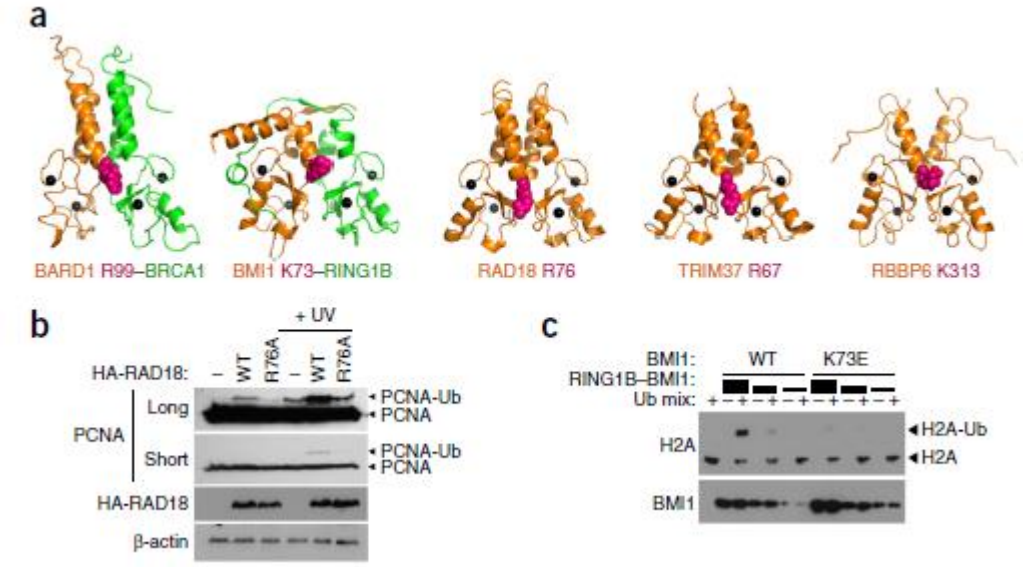

*Figure 2 Other type 1 RING E3 ligases require arginine or lysine residues on the partner protomer. (**a**) Structural models showing views in the same orientation of type 1 RING–RING structures: BRCA1–BARD1 (PDB 1JM7 (ref. 18)) with BMI1–RING1B (PDB 2CKL (ref. 40)), RAD18 (PDB 2Y43 (ref 41)), TRIM37 (PDB 3LRQ) and RBBP6 (PDB 3ZTG (ref. 42)). Residues equivalent to R99 of BARD1 are shown in pink. (**b**) Western blot showing loss of the ability to induce monoubiquitination of PCNA after R76A RAD18 expression. Samples are cells transfected with either WT RAD18 or R76A RAD18 mutant in otherwise untreated HEK293 cells or those treated with 40 J UV. Lysates were probed for PCNA and controls as indicated. (**c**) Western blots indicating monoubiquitination of H2A in nucleosomes by incubation with WT BMI1–RING1B or K73E BMI1–RING1B heterodimers. Uncropped blot images are shown in **Supplementary Data Set 1**.*

Ligase activity is required for a subset of BRCA1 responses

To address possible roles of the BRCA1–BARD1 Ub ligase activity, we depleted HeLa cells of endogenous BARD1 and expressed short interfering RNA (siRNA)-resistant full-length WT BARD1 cDNA or mutant forms bearing BARD1 amino acid substitutions R99E or L44R (illustrated in **Fig. 3a**). L44R introduces a large hydrophilic residue in the hydrophobic helical face of BARD1, thereby preventing interaction with BRCA1 (ref. 20). Complementation of cells with L44R BARD1 did not support heterodimer formation or heterodimer stability, or promote endogenous BRCA1 localization to irradiation-induced foci (IRIF) (**Supplementary Fig. 3a–c**). In contrast, R99E BARD1 retained dimerization with BRCA1 and promoted both BRCA1 stability and localization to IRIF (**Supplementary Fig. 3a–c**). Purified complexes of neither R99E BARD1 nor L44R BARD1 exhibited Ub ligase activity (**Supplementary Fig. 3d**). Thus, L44R BARD1

disrupts both heterodimer formation and ligase activity in cells, whereas the R99E BARD1 variant is ligase defective but promotes heterodimer formation.

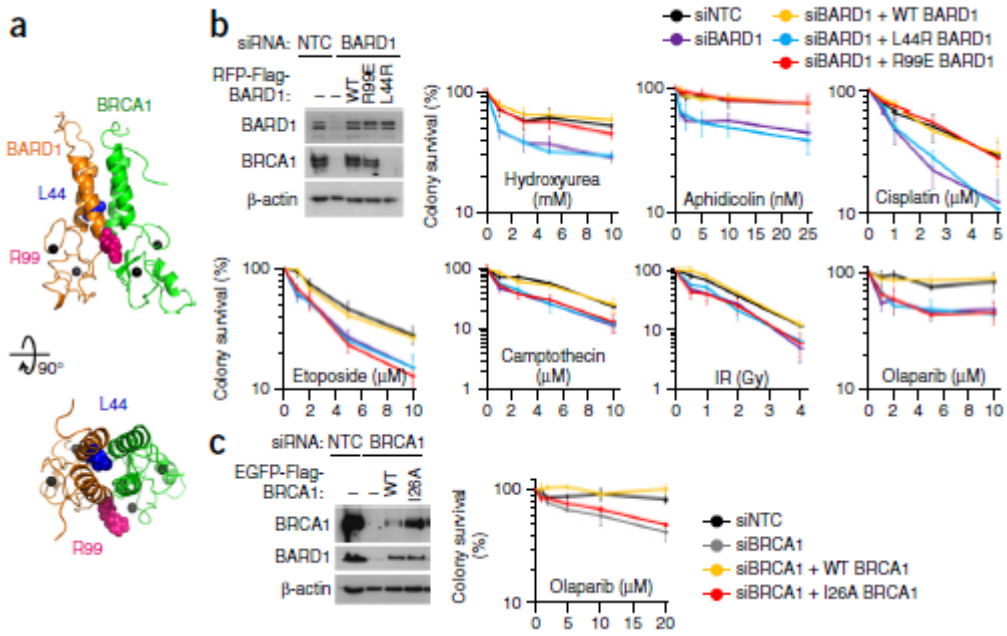

*Figure 3 BRCA1–BARD1 ligase activity promotes survival after exposure to certain DNA-damaging agents. (**a**) Structural model of BARD1 (orange) and BRCA1 (green) (PDB 1JM7 (ref. 18)) illustrating the location of L44 (blue) and R99 (pink). Zinc ions are filled spheres (black). The lower image is a 90° rotation about the horizontal. (**b**) Immunoblot of cells treated with nontargeting control siRNA (siNTC) or BARD1 siRNA (siBARD1) and complemented with the siRNA-resistant BARD1 variants shown. The graphs show cell survival, relative to that of NTC control, of cells depleted and complemented in this way, exposed to the agents shown, plated and counted 10–14 d later. Colony numbers are expressed as a percentage of the colony numbers of untreated cells. Means ± s.e.m. from 3–6 independent experiments are shown (Source Data available online). (**c**) As in **b**, depleted with BRCA1 siRNA (siBRCA1) and complemented with siRNA-resistant WT BRCA1 and I26A BRCA1. Means ± s.e.m. from 4 or 5 independent experiments are shown (Source Data available online). Uncropped blot images are shown in **Supplementary Data Set 1**.*

To differentiate potential roles of ligase activity from those of the heterodimer in DNA repair, we compared the survival of cells depleted of endogenous BARD1 and complemented with the separation-of-function variants in response to various DNA-damaging agents. BARD1 depletion or complementation with L44R BARD1 resulted in sensitivity to each DNA-damaging agent tested, and complementation with the WT BARD1 protein restored resistance (**Fig. 3b**). Strikingly R99E BARD1–complemented cells exhibited resistance to some agents but not to others. They were resistant to agents that stall or slow replication forks (hydroxyurea (HU) and aphidicolin) and to the intrastrand-cross-linking agent cisplatin, but they were sensitive to camptothecin (a topoisomerase I poison), etoposide (a topoisomerase II poison), olaparib (AZD-2281, an inhibitor of poly(ADP-ribose) polymerase) and irradiation (**Fig. 3b**). These data prompted us to revisit the I26A substitution of BRCA1 that disrupts interaction with E2 conjugating enzymes (ref. 7 and **Supplementary Fig. 3e**). Cells depleted of endogenous BRCA1

and complemented with I26A BRCA1 were also sensitive to olaparib (**Fig. 3c**), thus supporting the notion that the BRCA1–BARD1 Ub ligase activity supports olaparib resistance.

Ligase activity promotes 53BP1 repositioning and resection

The sensitivities of ligase-defective cells suggest a role in the promotion of HR, a process begun by resection of DNA ends. To interrogate the HR pathway, we first examined the single-stranded DNA–binding protein replication protein A (RPA), which forms foci after irradiation and is indicative of resection. Cells complemented with R99E BARD1 or L44R BARD1 exhibited decreased numbers, size and intensity of RPA foci and also exhibited decreased foci of the human homolog of yeast radiation mutant 51 (RAD51), compared with those in WT BARD1–complemented cells (**Fig. 4a** and **Supplementary Fig. 4a**). These data suggest that ligase activity relates to the role of BRCA1 in promoting DNA resection before formation of the RAD51 nucleofilament in HR.

53BP1 and its effector proteins block DNA resection in the absence of BRCA1 (ref. 4). As anticipated, depletion of 53BP1 alleviated the requirement for BRCA1–BARD1 Ub ligase activity in olaparib and camptothecin resistance, increased RAD51 and RPA foci after irradiation and improved repair of an integrated HR substrate in a manner dependent on the CtBP-interacting protein and nuclease (CtIP) (**Fig. 4b** and **Supplementary Fig. 4b–f**). Depletion of the 53BP1 effector proteins, human REV7 (also known as MAD2 mitotic arrest deficient–like 2 (MAD2L2))[21,22] or Artemis[23] similarly improved survival of R99E BARD1–complemented cells after treatment with irradiation, olaparib or camptothecin to differing degrees, depending on the agent (**Supplementary Fig. 5a–c**).

These data provide what is, to our knowledge, the first evidence that the Ub ligase activity of BRCA1–BARD1 contributes to the function of BRCA1 in DNA resection and, consistently with the described relationship between BRCA1 and 53BP1, it can be bypassed by loss of 53BP1 or its effector proteins. In contrast, the resistance of BRCA1-depleted cells to HU was not restored by 53BP1 depletion (**Fig. 4c**), a result consistent with the notion that the Ub-ligase-independent functions of BRCA1 do not include interaction with 53BP1.

The recruitment of BRCA1 into the core of IRIF is associated with the eviction of 53BP1 to the periphery of the foci and the concurrent RPA recruitment to the core[24,25]. We measured the distribution of 53BP1 in foci associated with BRCA1 in BARD1-depleted cells complemented with WT or R99E BARD1 protein. Whereas the distribution of BRCA1 within IRIF in these cells was similar, the cells complemented with R99E BARD1 showed markedly decreased eviction of

53BP1 to the periphery (**Fig. 4d**). Thus, the ligase activity plays a role in 53BP1 repositioning at IRIF.

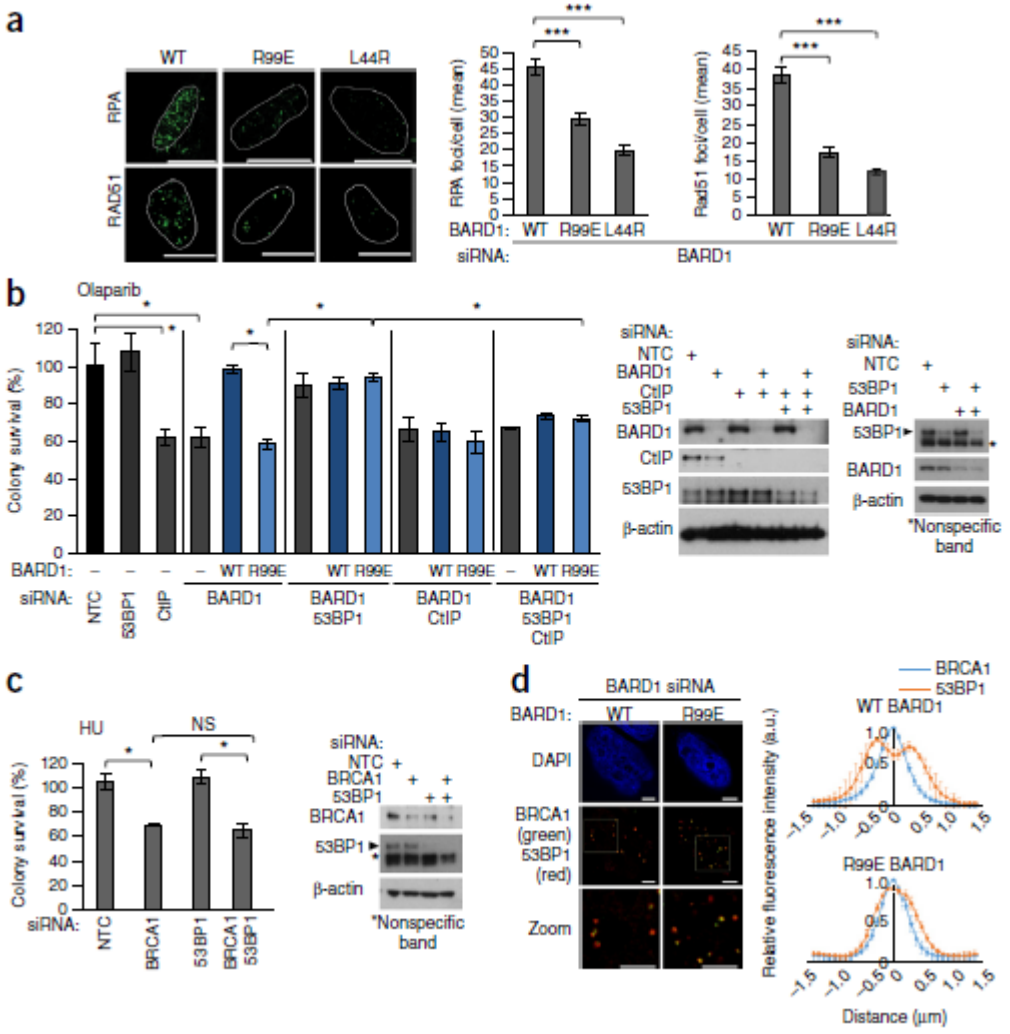

*Figure 4 BRCA1–BARD1 ligase activity promotes DNA resection in the presence of 53BP1. (**a**) RPA and RAD51 foci in 5-ethynyl-2′-deoxyuridine (EdU)-positive cells treated with BARD1 siRNA and complemented with siRNA-resistant WT, R99E or L44R BARD1 variants. Micrographs show representative cells; scale bars, 10 μm. Graphs show mean number of foci per cell; error bars, s.e.m. (RPA, 60 cells; Rad51, 100 cells). (**b**) Colony cell survival after olaparib (10 μM) treatment, relative to NTC control, of cells treated with BARD1 siRNA and complemented with WT or R99E BARD1 and treated with the additional indicated siRNAs. Graphs show means ± s.e.m. from four independent experiments. Western blots show detection of BARD1, CtIP and 53BP1 in treated cells. (**c**) Colony survival of BRCA1-depleted cells and cells co-depleted with 53BP1 and treated with HU (3 mM), compared with NTC-treated controls. Graph shows means ± s.e.m. from three independent experiments. Western blots show detection of 53BP1 and BRCA1 in treated cells. (**d**) High-resolution images of BRCA1 and 53BP1 in cells treated with BARD1 siRNA and complemented with WT or R99E BARD1, exposed to 2 Gy irradiation and fixed 8 h later. Scale bars, 10 μm. Graphs show an average across 30 profiles, over three experimental repeats; error bars, s.d. A.u., arbitrary units. For **a**–**c**, ***P < 0.005; *P < 0.05; NS, not significant by two-sided Student's t test. Source Data for graphs are available online.*

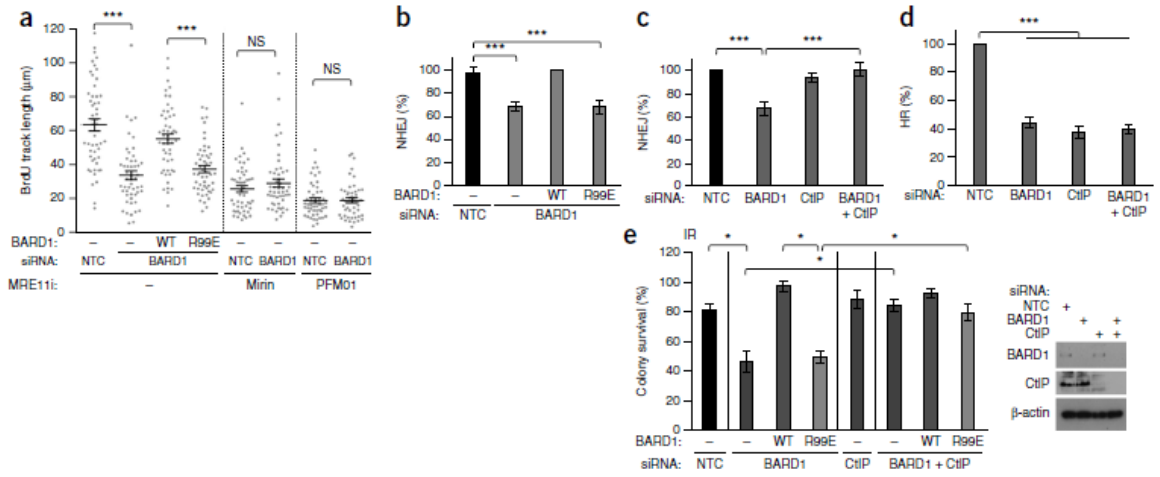

*Figure 5 BRCA1–BARD1 ligase activity is required after HR commitment. (**a**) BrdU track lengths in cells treated with BrdU and olaparib (10 μM) and MRN inhibitors. Horizontal line, mean; error bars, s.e.m. (n = 50 fibers measured per condition); Source Data are available online. (**b**) Quantification of GFP recovery in NHEJ-substrate cells depleted of BARD1 and transfected with siRNA-resistant variants. Means ± s.e.m. from four independent experiments are shown. (**c**) Quantification of GFP recovery in NHEJ-substrate cells depleted of BARD1, CtIP or both. Means ± s.e.m. from six independent experiments are shown. (**d**) Quantification of GFP recovery in HR-substrate cells depleted of BARD1, CtIP or both. Means ± s.e.m. from six independent experiments are shown. (**e**) Colony survival of cells treated with irradiation (0.5 Gy) and depleted of BARD1 and complemented with WT or R99E BARD1 or co-depleted of BARD1 and CtIP, relative to survival of control treated cells. Graph shows means ± s.e.m. from three independent experiments. Source Data for graphs are available online. Western blots show detection of BARD1, CtIP and β-actin. Uncropped blot images are shown in **Supplementary Data Set 1**. Throughout figure, ***P < 0.005; *P < 0.05 NS, not significant by two-sided Student's t test.*

Ligase activity in resection is needed after HR commitment

Resection consists of an initiation step, requiring the nuclease CtIP and meiotic recombination 11 homolog A (MRE11) endonuclease activity, and an elongation stage, requiring MRE11 exonuclease activity and then extension by exonuclease 1 (EXO1) or Bloom Syndrome RecQ helicase (BLM) and DNA replication helicase/nuclease 2 (DNA2) (reviewed in ref. 26). To assess when the BRCA1–BARD1 Ub ligase activity is required in resection, we incubated cells with bromodeoxyuridine (BrdU) and then measured track lengths of the exposed BrdU epitope, which were indicative of single-stranded DNA as a measure of resected DNA after olaparib exposure (as described in ref. 27). R99E BARD1–complemented cells or BARD1-depleted cells showed shorter resection lengths, which were similar to those of cells exposed to the MRE11 exonuclease inhibitor MIRIN but were not as severely truncated as those in cells exposed to the MRE11 endonuclease inhibitor PFM01 (**Fig. 5a**). These data suggest that some resection occurs in BRCA1–BARD1 ligase–defective cells after the requirement for MRE11 endonuclease activity.

Incomplete resection after commitment results in irradiation sensitivity, which is largely rescued by the inhibition of resection initiation through CtIP depletion, because loss of CtIP

prevents HR commitment but allows repair by NHEJ28. We found that depletion of CtIP improved the repair of an NHEJ substrate but not an HR substrate in BARD1-depleted cells (**Fig. 5b–d**) and restored the majority of the resistance of R99E BARD1–complemented or BARD1-depleted cells to irradiation (**Fig. 5e**). These data functionally confirm that the requirement for BRCA1 ligase activity occurs after HR commitment. They also suggest that in BRCA1–BARD1-deficient cells, or in cells lacking its Ub ligase function, most sensitivity to irradiation is a consequence of incomplete resection and poor NHEJ, and a smaller proportion is due to HR deficiency.

An H2A-Ub fusion promotes DNA resection

We next assessed possible targets of BRCA1–BARD1 ubiquitination including 53BP1, its effector proteins and histones. We irradiated cells transfected with constructs expressing histidine-Myc-tagged Ub and BARD1 and purified covalently bound Ub conjugates under highly denaturing conditions. 53BP1 and H2A were enriched in WT BARD1–expressing cells but were decreased in cells expressing R99E BARD1 mutants (**Fig. 6a**), thus suggesting that BRCA1–BARD1 E3 ligase activity results in ubiquitination of these two proteins. H2A modification was visible in the R99E BARD1 lane after high exposure, thus indicating an additional, expected, BRCA1–BARD1-independent modification.

H2A has previously been identified as a BRCA1–BARD1 Ub ligase target[8,9,17], where it is modified at its C-terminal lysines K125, K127 and K129 (ref. 8). We attempted to replace a proportion of endogenous H2A (which is expressed from several genes) with mutant histone by generating stable cell lines bearing H2A K125R, K127R and K129R mutations. However, the expression of the H2A mutants had no effect on olaparib sensitivity, thus suggesting either that modification elsewhere is important for resistance or that insufficient mutant histone incorporation was achieved (**Supplementary Fig. 6a**,**b**).

As an alternative approach, we generated a H2A mutant–Ub fusion protein and determined whether it could complement BARD1-depleted cells. In the H2A fusion, we mutated lysines 13, 15, 118, 119, 125, 127 and 129 to arginines to interrogate the function of the fused Ub in the absence of endogenous ubiquitination events; we also mutated the Ub itself at all seven lysines to prevent chain formation. Both exogenous H2A and the H2A-Ub fusion were incorporated into chromatin (**Fig. 6b**). In agreement with the previous finding that expression of a similar fusion improves repair of a gene-conversion substrate in BRCA1-deficent cells[9], we confirmed that expression of the H2A-Ub protein promoted repair of a gene-conversion substrate in BARD1-depleted cells (**Supplementary Fig. 6c,d**). To address whether H2A-Ub has the ability to

restore physiological HR, we examined the formation of RAD51 foci in BARD1-depleted cells. In a dose-response experiment, we found that H2A-Ub levels correlated with restoration of RAD51 foci, thus suggesting that greater incorporation of the protein into chromatin resulted in greater rescue (**Fig. 6c** and **Supplementary Fig. 6e**). Moreover, neither the degree of gene conversion nor the number of RAD51 foci in cells expressing H2A-Ub was further increased when 53BP1 was depleted (**Supplementary Fig. 6d**,**f**), thus indicating that H2A-Ub expression and the removal of 53BP1 had similar effects. Consistently with an ability to complement the lack of BRCA1–BARD1 ligase activity in HR, expression of H2A-Ub promoted the survival of BARD1-depleted cells after treatment with olaparib and camptothecin but did not restore the resistance

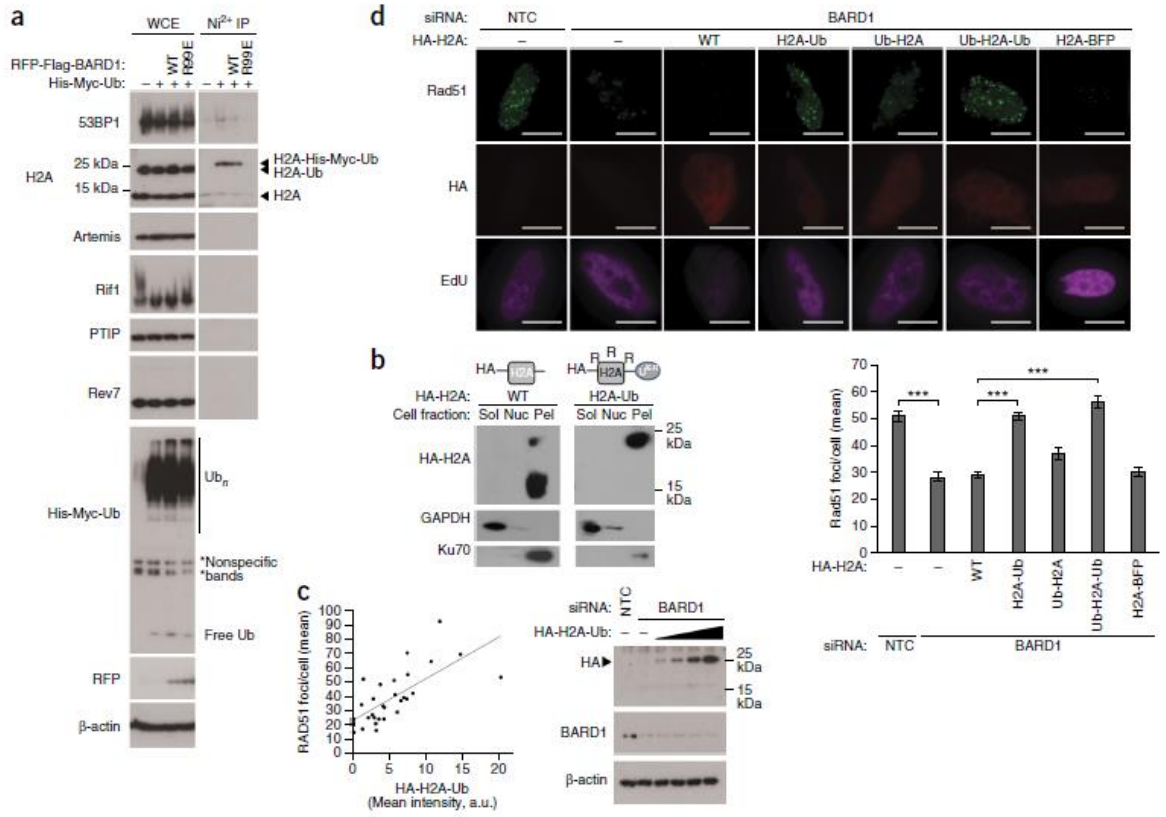

*Figure 6 BRCA1–BARD1-dependent modification of nucleosomes. (**a**) Western blot of selected proteins in whole cell extracts (WCE) and nickel-column immunoprecipitations (Ni^{2+} IP) of lysates from cells transfected with His-Myc-Ub and BARD1 constructs and irradiated (30 Gy). (**b**) Western blot of hemagglutinin (HA)-tagged H2A of cells transfected with HA-H2A or HA-H2A-Ub fusion. In the fusion, H2A carried lysine-to-arginine mutations at lysines 13, 15, 118, 119, 125, 127 and 129, and the seven lysines in the Ub were mutated to arginine (schematic at top). Cells were lysed sequentially in buffer containing increasing amounts of salt. Sol, soluble fraction; nuc, nuclear fraction; pel, pellet. (**c**) Quantification of HA-H2A-Ub intensity by ImageJ (expression), showing correlation with the number of RAD51 foci in BARD1-depleted S-phase cells after exposure to irradiation (5 Gy) and 2 h recovery (representative immunofluorescence images in **Supplementary Fig. 6e**); 30 cells were analyzed. Western blots show detection of BARD1 and HA-H2A-Ub expression in treated cells. (**d**) Staining of cells with RAD51, HA and EdU labeled S-phase cells. Scale bars, 10 μm. Graphs show quantification of RAD51 foci in BARD1-depleted cells expressing HA-H2A or various fusions of H2A and pulsed with EdU, fixed 2 h after 5 Gy IR. Means ± s.e.m. from 3 independent experiments are shown. n values (number of cells) are as follows: NTC (148), BARD1 siRNA (83), BARD1 siRNA + H2A (158), BARD1 siRNA + H2AUb (78), BARD1 siRNA + UbH2A (101), BARD1 siRNA + UbH2AUb (115), BARD1 siRNA + H2ABFP (129). ***P < 0.005 by two-sided Student's t test. Uncropped blot images are shown in **Supplementary Data Set 1**. Source Data for graphs are available online.*

to HU (**Supplementary Fig. 6g–i**), a result consistent with the requirement for BRCA1–BARD1 ligase activity. As anticipated, both the drug resistance and restoration of RAD51 conferred by H2A-Ub required CtIP (**Supplementary Fig. 6j**,**k**). Together, these data provide strong evidence that the H2A-Ub fusion restored physiological resection and HR in the BARD1-depleted cells.

We then examined the specifics of the H2A-Ub fusion in more detail. We tested an alternative globular protein, blue fluorescent protein (BFP), fused to the C terminus of H2A. This fusion was unable to rescue drug resistance or restore RAD51 foci in BARD1-depleted cells (**Fig. 6d** and **Supplementary Fig. 6g**,**i**) thus indicating that not all C-terminal protein fusions were able to complement. We addressed whether the location of the Ub might be critical and compared H2A (again bearing K-to-R mutations at positions 13, 15, 118, 119, 125, 127 and 129) in which Ub had been fused to the N terminus, the C terminus or both termini. The N-terminal fusion of Ub to H2A slightly improved the numbers of RAD51 foci in BARD1-deleted cells, whereas RAD51 foci in cells expressing H2A with Ub fused to the C terminus or to both ends were fully restored (**Fig. 6d**). These data suggest that a C-terminal Ub fusion is most able to promote formation of RAD51 foci and that Ub fused to the N terminus does not inhibit the restoration of HR promoted by the C-terminal fusion. Together, these data indicate that incorporation of H2A-Ub into chromatin either supports a function similar to that of the BRCA1–BARD1 ligase or contributes an indirect role that overcomes the need for heterodimer activity.

We next addressed how BRCA1–BARD1 ligase activity or Ub-modified nucleosomes might affect 53BP1 and resection. We assessed whether H2A-Ub fusions inhibit 53BP1 accumulation to IRIF, whether BRCA1–BARD1 depletion results in expression of epigenetically silenced genes or whether depletion of a repressive chromatin factor (chromodomain helicase DNA binding protein 3 (CHD3), part of the repressive nucleosome-remodeling deacetylase complex) might relieve the requirement for BRCA1–BARD1 (**Supplementary Fig. 7a–f** and **Supplementary Note**). These potential mechanisms were not supported by evidence from our investigations.

SMARCAD1 is part of the BRCA1–BARD1 ligase pathway

We then focused on the proteins involved in the later stages of DNA resection and observed decreased BLM recruitment to IRIF in BARD1-depleted cells (**Supplementary Fig. 7g**). Unlike the requirement for BRCA1–BARD1 ligase activity, the requirement for late-stage resection enzymes in HR cannot be overcome by a loss of 53BP1 (refs. 29,30), thus leading us to consider the phenomenon of poor BLM recruitment as an indication of a defect occurring earlier in the process.

In yeast, the ATP-dependent chromatin remodeler function unknown now 30 (Fun30) promotes the activity of Exo1 and Sgs1 (BLM) in resection[31–33]. The mammalian homolog SMARCAD1 also promotes resection[32], and the protein has two Ub-binding CUE domains (which are similar to a domain in the yeast Cue1 protein)[34] (**Fig. 7a**). To test whether this protein might link BRCA1–BARD1-dependent chromatin modification to 53BP1 repositioning and DNA resection, we examined the interaction of the SMARCAD1 CUE domains with nucleosomes bearing H2A-Ub. Nickel beads bound to hexahistidine (His_6)-tagged SMARCAD1 CUE domains pulled down H2A-Ub but not H2A, whereas SMARCAD1 CUE-domain mutants (termed CUEm, with Ub-contacting phenylalanine, alanine and leucine residues, as previously described35, changed to glutamate) purified neither histone (**Fig. 7b**).

We next addressed SMARCAD1 recruitment and introduced siRNA-resistant plasmids encoding full-length SMARCAD1 or CUEm SMARCAD1 into SMARCAD1-depleted cells (**Fig. 7c**). WT SMARCAD1 localized to laser-induced sites of DNA damage decorated with phosphorylated histone H2AX (γ-H2AX) (**Fig. 7d**). Its accumulation was decreased, but not lost, when BARD1 was depleted. Similarly the CUE mutant, compared with the WT protein, showed decreased intensity at laser-induced sites of damage (**Fig. 7d**). The recruitment of CUEm SMARCAD1 was not further decreased by depletion of BARD1, thereby suggesting that BARD1 and the CUE domains affect SMARCAD1 accumulation through the same pathway (**Fig. 7d**). Pretreatment of cells with KU55933, a specific inhibitor ATM36, substantially diminished the formation of γ-H2AX from the path of the laser line, and it also sustainably decreased SMARCAD1 accumulation (**Fig. 7d**). Thus, although BRCA1–BARD1 and SMARCAD1 CUE domains support SMARCAD1 recruitment, other ATM-dependent events are also required.

We further tested the relationship between BRCA1–BARD1 and SMARCAD1. We found that although SMARCAD1 depletion alone decreased drug resistance and HR, this effect was not more pronounced in cells also lacking BRCA1–BARD1 activity (**Supplementary Fig. 8a**,**b**), thus suggesting that SMARCAD1 and BRCA1–BARD1 ligase activity influence drug resistance through the same pathway. Moreover H2A-Ub expression was unable to restore RAD51 foci levels in BARD1-depleted cells that were also depleted of SMARCAD1 (**Supplementary Fig. 8c**). This evidence suggests a requirement for SMARCAD1 downstream of BRCA1–BARD1 ligase activity and C-terminal H2A ubiquitination. From these data, we predicted that SMARCAD1 and BRCA1–BARD1 have similar functions in resection and HR, and we therefore examined the relationship with 53BP1 in resection and in IRIF. Loss of 53BP1 restored full BrdU resection lengths to

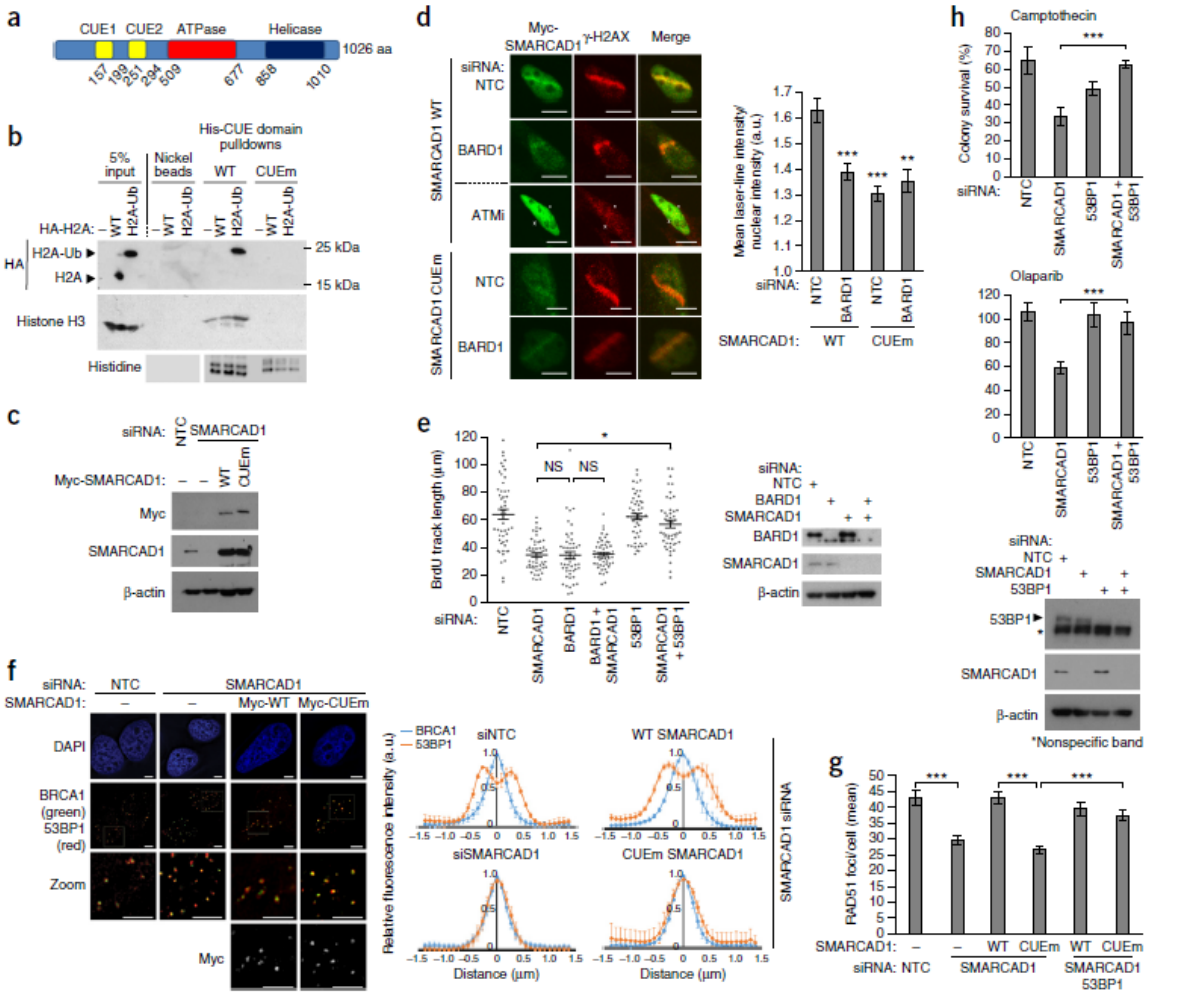

Figure 7 The nucleosome remodeler SMARCAD1 is in the pathway including BRCA1–BARD1 ligase activity. ***(a)*** *SMARCAD1 domain architecture.* ***(b)*** *Western blot of HA-H2A (WT) or H2A-Ub expressed in cells and bound to purified WT or mutant SMARCAD1 CUE domains (aa 98–318).* ***(c)*** *Western blot showing expression of full-length WT and CUE-domain-mutant SMARCAD1 in SMARCAD1-depleted cells.* ***(d)*** *Representative images of cells expressing siRNA-resistant SMARCAD1 variants treated with SMARCAD1 siRNA or co-depleted with BARD1 siRNA and bearing laser-line-induced DNA damage. Scale bars, 10 μm. ATMi, treatment with 10 μM KU55933 ATM inhibitor 4 h before damage. White 'X' marks the laser-line path. Graph shows the intensity of myc-SMARCAD1 measured in the region of the γ-H2AX laser line, compared with nucleoplasm A.u., arbitrary units Means ± s.e.m. are shown; n values (number of cells) are as follows: NTC siRNA + myc-SMARCAD1 WT (50), BARD1 siRNA + myc-SMARCAD1 WT (63), NTC siRNA + myc-SMARCAD1 CUEm (43), BARD1 siRNA + myc-SMARCAD1 CUEm (23). **P < 0.01; ***P < 0.005 by Student's t test.* ***(e)*** *Lengths of BrdU DNA fibers after treatment with olaparib (10 μM) in cells treated with the siRNAs shown. Data shown are 50 fibers per condition, with means ± s.e.m. *P < 0.05 NS, not significant by two-sided Student's t test. Western blots of BARD1 and SMARCAD1 in treated cells are shown.* ***(f)*** *Representative images of cells transfected with siRNA targeting SMARCAD1 with siRNA-resistant WT and CUEm myc-SMARCAD1 exposed to 2 Gy irradiation and fixed 8 h later. Scale bars, 10 μm. Graphs show averages of 30 foci profiles; error bars, s.d.* ***(g)*** *Quantification RAD51 foci in cells transfected with SMARCAD1 and 53BP1 siRNA together with siRNA-resistant forms of SMARCAD1. Means ± s.e.m. are shown; n values (number of cells) as follows: NTC (92), SMARCAD1 siRNA (71), SMARCAD1 siRNA + myc-SMARCAD1 WT (76), SMARCAD1 siRNA + myc-SMARCAD1 CUEm (92), SMARCAD1 53BP1 siRNA + myc-SMARCAD1 WT (74), SMARCAD1 53BP1 siRNA + myc-SMARCAD1 CUEm (92). ***P < 0.005 by two-sided Student's t test.* ***(h)*** *Colony cell survival after treatment with olaparib (10 μM) or camptothecin (2.5 μM), and untreated controls of SMARCAD1-complemented cells. Mean ± s.e.m. from 3–7 independent experiments are shown. ***P < 0.005 by two-sided Student's t test. Western blots show SMARCAD1 and 53BP1 in treated cells. Uncropped blot images are shown in* ***Supplementary Data Set 1****. Source Data for graphs are available online.*

SMARCAD1-depleted cells (**Fig. 7e**), thus suggesting that an antagonistic relationship between SMARCAD1 and 53BP1 regulates resection. Moreover, in S-phase or G2-phase SMARCAD-depleted cells, we observed that 53BP1 was not evicted to the periphery of BRCA1-associated foci, a result indicating that SMARCAD1 is also required for 53BP1 repositioning (**Fig. 7f**). Expression of an siRNA-resistant WT SMARCAD1 protein restored normal distribution of 53BP1, but expression of the CUEm SMARCAD1 or an ATPase-dead form (K528R) did not (**Fig. 7f** and **Supplementary Fig. 8d**), thus indicating that both the CUE domains and enzymatic activity are required for repositioning 53BP1. Because the effect was not partial, these data also suggest that the CUE domains have a role in promoting 53BP1 repositioning beyond supporting the accumulation of SMARCAD1 at sites of damage.

In complementation of cells depleted of endogenous SMARCAD1, we found that CUEm SMARCAD1 was unable to restore RAD51 foci in irradiation-treated cells, and neither CUEm SMARCAD1 nor the ATPase-dead-mutant form restored the olaparib or camptothecin resistance of SMARCAD1-depleted cells (**Fig. 7g** and **Supplementary Fig. 8e**). Thus, the SMARCAD1 CUE domains are essential to promoting HR, consistently with their role in 53BP1 repositioning and drug resistance. As anticipated, the need for the SMARCAD1 CUE domains in promoting HR, as measured by RAD51 IRIF formation, was bypassed by treatment with siRNA to 53BP1 (**Fig. 7g**). Similarly the repression of 53BP1 restored cellular olaparib and camptothecin resistance in SMARCAD-depleted cells (**Fig. 7h**), thus confirming that SMARCAD1 is less important to cell survival when 53BP1 is absent. Together, these data confirm a link between BRCA1–BARD1 and SMARCAD1 in promoting resection in the presence of 53BP1.

DISCUSSION

Our data provided insight into how BRCA1 inhibits the 53BP1-complex-mediated block on resection. The BRCA1–BARD1 Ub ligase promotes a subset of DNA-repair functions attributed to BRCA1 and participates in promoting resection steps after CtIP- and MRE11-mediated commitment to HR. Consistently with the restoration of HR in BRCA1–BARD1 deficient cells, our results suggested that H2A-Ub complementation functions at the level of resection restoration. Initially we were surprised that our data indicated that C-terminal Ub modification of H2A is unlikely to directly inhibit the 53BP1 interactions. Instead, we found that promotion of HR requires the Ub-binding CUE domains of the chromatin remodeler SMARCAD1. Critically, both BRCA1 ligase activity and SMARCAD1 reposition 53BP1 within IRIF, and this repositioning correlates with the promotion of resection.

Our data suggest a model in which the BRCA1–BARD1 ligase modifies chromatin, thereby promoting the accumulation and activity of the chromatin remodeler SMARCAD1, which then mobilizes 53BP1 and allows the completion of resection (**Fig. 8**). We suggest that BRCA1 activity, through this mechanism, promotes HR and inhibits toxic end-joining. Our model does not exclude an additional role for the observed 53BP1 ubiquitination, but notably H2A-Ub is sufficient to restore HR to near-normal levels in BRCA1–BARD1-deficient cells.

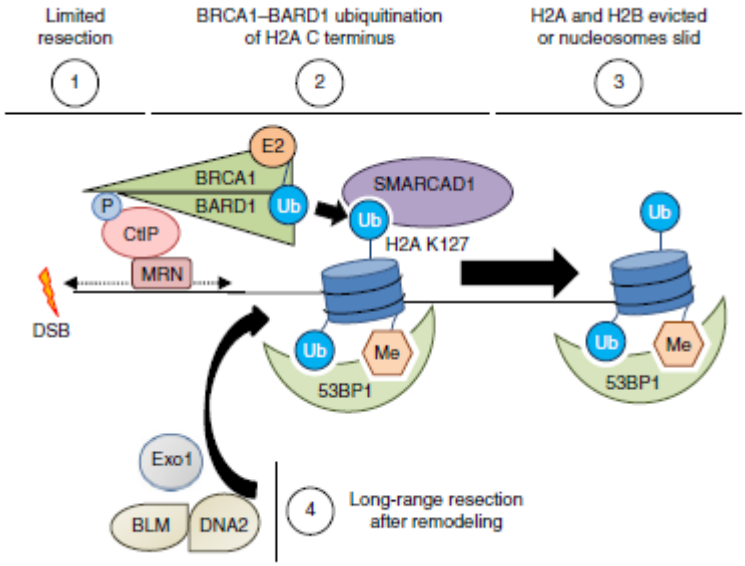

Figure 8 Proposed model for the BRCA1–BARD1 Ub ligase in promoting resection at DSB-damaged chromatin. (1) Limited resection occurs in the absence of BRCA1–BARD1 activity, in a manner dependent on CtIP–Mre11. (2) BRCA1–BARD1-dependent Ub modification of H2A promotes SMARCAD1 interaction with damage-proximal nucleosomes. (3) SMARCAD1 activity repositions or evicts nucleosomes, and moves 53BP1 and its effector proteins, thereby releasing 53BP1-mediated inhibition of DNA resection. (4) Long-range resection can proceed. Me, methyl; P, phospho-.

Yeast Fun30 can both slide nucleosomes and evict histone H2A and H2B dimers [37,38]; hence, whether SMARCAD1 shunts or removes DNA-damage-proximal histones is not yet known. Conceptually, nucleosome sliding may be inhibited by upstream nucleosomes, and eviction is a simpler model. In yeast, histones remain bound to DSB ends for a longer amount of time in *fun30*Δ cells[31]. In either case, remodeled nucleosomes may be those loaded with 53BP1 or may become refractory to 53BP1 interaction. SMARCAD1 is also required in the reestablishment of silent heterochromatin after DNA replication[39]. It will be intriguing to determine whether decreased SMARCAD1 activity at chromatin contributes to the decreased heterochromatin observed in Brca1-deficient mouse cells[9].

We showed that cell survival in response to some DNA-damaging agents requires BRCA1 ligase function to counter 53BP1, whereas the responses to other agents, which induce replicative stress or intrastrand cross-links, are independent of this pathway. This information may provide a rationale for tailored anticancer treatment for some *BRCA1*-mutation carriers, because targeting ligase-dependent and ligase-independent aspects of the BRCA1 defect would be expected to slow the development of tumor resistance through 53BP1-complex downregulation or mutation.

Several *BRCA1* missense variants occur in the N terminus and have the potential to disrupt E3 Ub ligase function[16]. The role identified here for the ligase activity in promoting HR suggests a possible role in cancer protection. In defining the Ub-priming face of this and other type 1 E3 Ub ligases, our data provide a robust new means by which the ligase function can be assessed in cells and organisms.

Methods

Methods and any associated references are available in the online version of the paper.

Note: Any Supplementary Information and Source Data files are available in the online version of the paper.

Acknowledgments

Grant funding for this project was as follows. CRUK: C8820/A19062 (R.M.D., A.G., H.R.S. and J.B.), C302/A14532 and C1206/A11978 (F.Z.W. and L.H.P.); Breast Cancer Campaign: 2010MayPR01 (J.S.) and 2013NovPR132 (S.B.-R.); Engineering and Physical Sciences Research Council EP/L016346/1 (R.N.); University of Birmingham (A.F., B.J. and R.M.D.); University of Sussex (R.A.B.); HEFCE (J.R.M., R.N. and N.H.K.). We thank J. Stark (City of Hope) for U20S-DR3 and U20S-EJ5 cells and the I-*SceI* plasmid; R. Everett (MRC Virology Unit, Glasgow) for UBE2D1 cDNA and the myc-His-ubiquitin construct; T. Sixma and M. van Lohuizen, (both NKI Netherlands) for the Ring1b159/Bmi1109 coexpression construct and BMI1-GFP; A. Zlatanou (University of Birmingham) for HA-Rad18; G. Stewart (University of Birmingham) for Flp-In HeLa cells and anti-MDC1 antibody; R. Katz (Fox Chase Cancer Center) for cryptic EGFP HeLa cells; and J. Tainer (Scripps Research Institute) for PFM01 inhibitor. Determination of the structure of the TRIM37 domain was supported by an NIH Protein Structure Initiative grant to G.T. Montelione, J.F. Hunt and the Northeast Structural Genomics Consortium. We thank R. Hay for useful discussions and T. Sixma and M. Uckelmann for insights into the contribution of H2A-Ub interactions in purified nucleosomes.

AUTHOR CONTRIBUTIONS

R.M.D. performed structural analysis, generated proteins, performed cell and biochemical experiments, designed experiments and interpreted data. A.J.G. generated constructs and cell lines, and performed colony survival experiments. H.R.S. performed resection experiments and fluorescence microscopy. J.S. generated BARD1 cell lines and performed immunoprecipitation experiments. R.A.B. performed high-resolution BRCA1 and 53BP1 microscopy and analysis. A.F. generated RING1B–BMI1 proteins and performed biochemistry. B.J. quantified foci. M.D.-M. generated BRCA1 cell lines. S.B.-R. and J.B. provided technical support and yeast experiments. L.H.P., R.N., N.H.K. and F.Z.W. provided supervisory help and data interpretation. J.R.M. and R.M.D. wrote the paper. A.J.G., H.R.S. and M.D.-M. commented on the paper and ongoing research. J.R.M. contributed to data interpretation and directed the project.

COMPETING FINANCIAL INTERESTS

The authors declare no competing financial interests.

REFERENCES

1. Long, D.T. & Walter, J.C. A novel function for BRCA1 in crosslink repair. *Mol. Cell* **46**, 111–112 (2012).
2. Schlacher, K., Wu, H. & Jasin, M. A distinct replication fork protection pathway connects Fanconi anemia tumor suppressors to RAD51-BRCA1/2. *Cancer Cell* **22**, 106–116 (2012).
3. Jiang, Q. & Greenberg, R.A. Deciphering the BRCA1 tumor suppressor network. *J. Biol. Chem.* **290**, 17724–17732 (2015).
4. Panier, S. & Boulton, S.J. Double-strand break repair: 53BP1 comes into focus. *Nat. Rev. Mol. Cell Biol.* **15**, 7–18 (2014).
5. Bunting, S.F. *et al.* 53BP1 inhibits homologous recombination in Brca1-deficient cells by blocking resection of DNA breaks. *Cell* **141**, 243–254 (2010).
6. Escribano-Díaz, C. *et al.* A cell cycle-dependent regulatory circuit composed of 53BP1-RIF1 and BRCA1-CtIP controls DNA repair pathway choice. *Mol. Cell* **49**, 872–883 (2013).
7. Brzovic, P.S. *et al.* Binding and recognition in the assembly of an active BRCA1/BARD1 ubiquitin-ligase complex. *Proc. Natl. Acad. Sci. USA* **100**, 5646–5651 (2003).
8. Kalb, R., Mallery, D.L., Larkin, C., Huang, J.T. & Hiom, K. BRCA1 is a histone-H2A-specific ubiquitin ligase. *Cell Rep.* **8**, 999–1005 (2014).
9. Zhu, Q. *et al.* BRCA1 tumour suppression occurs via heterochromatin-mediated silencing. *Nature* **477**, 179–184 (2011).

10. Sato, K. *et al.* A DNA-damage selective role for BRCA1 E3 ligase in claspin ubiquitylation, CHK1 activation, and DNA repair. *Curr. Biol.* **22**, 1659–1666 (2012).
11. Reid, L.J. *et al.* E3 ligase activity of BRCA1 is not essential for mammalian cell viability or homology-directed repair of double-strand DNA breaks. *Proc. Natl. Acad. Sci. USA* **105**, 20876–20881 (2008).
12. Drost, R. *et al.* BRCA1 RING function is essential for tumor suppression but dispensable for therapy resistance. *Cancer Cell* **20**, 797–809 (2011).
13. Plechanovová, A. *et al.* Mechanism of ubiquitylation by dimeric RING ligase RNF4. *Nat. Struct. Mol. Biol.* **18**, 1052–1059 (2011).
14. Dou, H., Buetow, L., Sibbet, G.J., Cameron, K. & Huang, D.T. Essentiality of a non-RING element in priming donor ubiquitin for catalysis by a monomeric E3. *Nat. Struct. Mol. Biol.* **20**, 982–986 (2013).
15. Metzger, M.B., Pruneda, J.N., Klevit, R.E. & Weissman, A.M. RING-type E3 ligases: master manipulators of E2 ubiquitin-conjugating enzymes and ubiquitination. *Biochim. Biophys. Acta* **1843**, 47–60 (2014).
16. Morris, J.R. *et al.* Genetic analysis of BRCA1 ubiquitin ligase activity and its relationship to breast cancer susceptibility. *Hum. Mol. Genet.* **15**, 599–606 (2006).
17. Mallery, D.L., Vandenberg, C.J. & Hiom, K. Activation of the E3 ligase function of the BRCA1/BARD1 complex by polyubiquitin chains. *EMBO J.* **21**, 6755–6762 (2002).
18. Brzovic, P.S., Rajagopal, P., Hoyt, D.W., King, M.C. & Klevit, R.E. Structure of a BRCA1–BARD1 heterodimeric RING–RING complex. *Nat. Struct. Biol.* **8**, 833–837 (2001).
19. Ismail, I.H., McDonald, D., Strickfaden, H., Xu, Z. & Hendzel, M.J. A small molecule inhibitor of polycomb repressive complex 1 inhibits ubiquitin signaling at DNA double-strand breaks. *J. Biol. Chem.* **288**, 26944–26954 (2013).
20. Morris, J.R., Keep, N.H. & Solomon, E. Identification of residues required for the interaction of BARD1 with BRCA1. *J. Biol. Chem.* **277**, 9382–9386 (2002).
21. Boersma, V. *et al.* MAD2L2 controls DNA repair at telomeres and DNA breaks by inhibiting 5′ end resection. *Nature* **521**, 537–540 (2015).
22. Xu, G. *et al.* REV7 counteracts DNA double-strand break resection and affects PARP inhibition. *Nature* **521**, 541–544 (2015).
23. Wang, J. *et al.* PTIP associates with Artemis to dictate DNA repair pathway choice. *Genes Dev.* **28**, 2693–2698 (2014).
24. Chapman, J.R., Sossick, A.J., Boulton, S.J. & Jackson, S.P. BRCA1-associated exclusion of 53BP1 from DNA damage sites underlies temporal control of DNA repair. *J. Cell Sci.* **125**, 3529–3534 (2012).

25. Kakarougkas, A. *et al.* Co-operation of BRCA1 and POH1 relieves the barriers posed by 53BP1 and RAP80 to resection. *Nucleic Acids Res.* **41**, 10298–10311 (2013).
26. Cejka, P. DNA end resection: nucleases team up with the right partners to initiate homologous recombination. *J. Biol. Chem.* **290**, 22931–22938 (2015).
27. Cruz-García, A., López-Saavedra, A. & Huertas, P. BRCA1 accelerates CtIP-mediated DNA-end resection. *Cell Rep.* **9**, 451–459 (2014).
28. Shibata, A. *et al.* Role of ATM and the damage response mediator proteins 53BP1 and MDC1 in the maintenance of G(2)/M checkpoint arrest. *Mol. Cell. Biol.* **30**, 3371–3383 (2010).
29. Tomimatsu, N. *et al.* Exo1 plays a major role in DNA end resection in humans and influences double-strand break repair and damage signaling decisions. *DNA Repair (Amst.)* **11**, 441–448 (2012).
30. Grabarz, A. *et al.* A role for BLM in double-strand break repair pathway choice: prevention of CtIP/Mre11-mediated alternative nonhomologous end-joining. *Cell Rep.* **5**, 21–28 (2013).
31. Chen, X. *et al.* The Fun30 nucleosome remodeller promotes resection of DNA double-strand break ends. *Nature* **489**, 576–580 (2012).
32. Costelloe, T. *et al.* The yeast Fun30 and human SMARCAD1 chromatin remodellers promote DNA end resection. *Nature* **489**, 581–584 (2012).
33. Eapen, V.V., Sugawara, N., Tsabar, M., Wu, W.H. & Haber, J.E. The *Saccharomyces cerevisiae* chromatin remodeler Fun30 regulates DNA end resection and checkpoint deactivation. *Mol. Cell. Biol.* **32**, 4727–4740 (2012).
34. Neves-Costa, A., Will, W.R., Vetter, A.T., Miller, J.R. & Varga-Weisz, P. The SNF2-family member Fun30 promotes gene silencing in heterochromatic loci. *PLoS One* **4**, e8111 (2009).
35. Shih, S.C. *et al.* A ubiquitin-binding motif required for intramolecular monoubiquitylation, the CUE domain. *EMBO J.* **22**, 1273–1281 (2003).
36. Hickson, I. *et al.* Identification and characterization of a novel and specific inhibitor of the ataxia-telangiectasia mutated kinase ATM. *Cancer Res.* **64**, 9152–9159 (2004).
37. Byeon, B. *et al.* The ATP-dependent chromatin remodeling enzyme Fun30 represses transcription by sliding promoter-proximal nucleosomes. *J. Biol. Chem.* **288**, 23182–23193 (2013).
38. Awad, S., Ryan, D., Prochasson, P., Owen-Hughes, T. & Hassan, A.H. The Snf2 homolog Fun30 acts as a homodimeric ATP-dependent chromatin-remodeling enzyme. *J. Biol. Chem.* **285**, 9477–9484 (2010).
39. Rowbotham, S.P. *et al.* Maintenance of silent chromatin through replication requires SWI/SNF-like chromatin remodeler SMARCAD1. *Mol. Cell* **42**, 285–296 (2011).

40. Buchwald, G. *et al.* Structure and E3-ligase activity of the Ring-Ring complex of polycomb proteins Bmi1 and Ring1b. *EMBO J.* **25**, 2465–2474 (2006).
41. Huang, A. *et al.* Symmetry and asymmetry of the RING-RING dimer of Rad18. *J. Mol. Biol.* **410**, 424–435 (2011).
42. Kappo, M.A. *et al.* Solution structure of RING finger-like domain of retinoblastoma-binding protein-6 (RBBP6) suggests it functions as a U-box. *J. Biol. Chem.* **287**, 7146–7158 (2012).

ONLINE METHODS

Constructs, primers, antibodies and reagents.

All constructs and mutations generated in house by site-directed mutagenesis were confirmed by sequencing (Source Biosciences). A full list of primers, siRNA sequences and antibodies used can be found in **Supplementary Tables 1–3**. Western blots show representative images taken from more than three independent experiments unless otherwise specified. All chemicals, unless otherwise stated, are from Sigma or Fisher.

Yeast two- and three-hybrid assays.

The yeast expression vectors used contained human BRCA1 N-terminal residues 2–300, expressed as a fusion with the transactivation domain VP16 (pVP16-BRCA1), and full-length E2 Ub-conjugating enzyme, human UBE2D1 or $BARD_{127–146}$, expressed as fusions with the DNA-binding protein LexA (pLexA). For three-hybrid studies, pY3H-Ade2 was generated from pY3H (Dualsystems Biotech) by cloning the Ade2 gene into Sbf1 and Stu1 sites, thus destroying the original Ura2 selection gene. Full-length BARD1 was cloned into the pY3H-Ade2 vector by Genscript. Growth on increasing concentrations of 3-AT, a competitive inhibitor of the product of the *HIS3* gene, indicates increased transcription of HIS3.

BRCA1–BARD1 protein production.

For bacterial expression of human BRCA1–BARD1 heterodimer, a bicistronic expression vector encoding His6-tagged BRCA11–300 and His_6-tagged $BARD1_{26–142}$ was generated by amplification of human *BRCA1* and *BARD1* cDNA templates and cloned into pET15b. Mutations were generated by site-directed mutagenesis of *BRCA1* or *BARD1*. Proteins were purified as described previously[16]. In brief, BRCA1 and BARD1 proteins were expressed in BL21(DE3) bacteria (Bioline). Bacteria were grown at 37 °C until an optical density of 0.6 was reached. Protein expression was induced by addition of 0.5 mM isopropyl β-D-1-thiogalactopyranoside (IPTG) (Bioline), and the temperature was immediately decreased to 25 °C. Bacteria were grown for a further 24 h. Bacterial pellets were collected after centrifugation at 3,000*g* for 10 min at 4 °C and then lysed in ice-cold lysis buffer (50 mM sodium phosphate, pH 7, 300 mM sodium chloride, 5% glycerol and 10 mM β-mercaptoethanol). Lysates were sonicated for 1 min at 30% intensity and then clarified by centrifugation at 14,000*g* for 10 min at 4 °C. The supernatant was incubated with 0.25 ml His-select beads (Sigma) overnight at 4 °C with rotation. The following day, the beads were washed with three 10-min washes in ice-cold wash buffer (50 mM sodium phosphate, pH 7, 300 mM sodium chloride, 5% glycerol, 10 mM β-

mercaptoethanol and 50 mM imidazole) before elution on ice in elution buffer (50 mM sodium phosphate, pH 7, 300 mM sodium chloride, 5% glycerol, 10 mM β-mercaptoethanol and 300 mM imidazole). Purified proteins were dialyzed against (25 mM Tris-HCl, pH 7.5, 10% glycerol, 2 mM dithiothreitol (DTT) and 150 mM potassium chloride), and purity was assessed by resolution on a 15% SDS–PAGE gel.

BMI1–RING1B protein production.

The $Ring1b_{159}$–$Bmi1_{109}$ construct (a kind gift from T. Sixma, NKI Netherlands) was coexpressed in *Escherichia coli* BL21(DE3) with both genes on a single promoter and a glutathione-S-transferase (GST)-fusion tag on the RING1B fragment only. After copurification on glutathione–Sepharose columns and washing, the dimer was eluted by cleavage with PreScission protease (as previously described[40]). Protein purity was assessed by resolution on a 15% SDS–PAGE gel.

Production of wild-type and D32R-Ub proteins.

Synthetic yeast ubiquitin was cloned into pGEX2TK before site-directed mutagenesis was performed to generate D32R. Constructs were expressed in BL21 cells (Bioline) and grown at 37 °C to an OD of 0.6 before protein expression was induced with 0.5 mM IPTG. Bacteria were grown for a further 16 h before lysis (20 mM Tris-HCl, pH 8, 130 mM sodium chloride, 1 mM EGTA, 1.5 mM magnesium chloride, 1% Triton X-100, 10% glycerol, 1 mM DTT and protease inhibitors (Complete Protease Inhibitor tablets, Roche). The lysate was sonicated for 1 min at 30% intensity and then clarified by centrifugation at 14,000*g* for 10 min at 4 °C. The supernatant was incubated with 0.25 ml glutathione–Sepharose-4B beads (GE Healthcare) overnight at 4 °C with rotation. The following day, the beads were washed with three ten-minute washes in ice-cold lysis buffer before a final wash in thrombin cleavage buffer (20 mM Tris, pH 8.4, 150 mM sodium chloride and 2.5 mM calcium chloride) was performed. Ubiquitin was eluted from the beads by cleavage of the GST tag with 2 U thrombin (Promega) overnight at 4 °C. The following day, the supernatant was incubated with 50 µl *p*-aminobenzamidine-agarose (Sigma) for 2 h to remove thrombin before dialysis against (25 mM Tris-HCl, pH 7.5, 10% glycerol, 2 mM DTT and 150 mM potassium chloride).

SMARCAD1 CUE-domain protein production and pulldowns.

Codon-optimized SMARCAD1 CUE domains (aa 98–318) WT and CUEm (L168E F169E L195E L196E F263E A285E L286E) were custom synthesized by Genscript and cloned into pET15b. The CUE domains were expressed in BL21(DE3) bacteria and purified on nickel beads, as described for BRCA1–BARD1 protein production. Nickel beads bound by CUE domains were stored in PBS for short-term pulldown experiments.

Lysates were prepared from HeLa Flp-In stable cell lines (empty, HA-H2A or HA-H2A-Ub cell lines) which had been induced with doxycycline (1 μg/ml) for 72 h to allow protein expression and chromatin incorporation of the HA-H2A constructs. Cells were lysed in 20 mM Tris, pH 8, 137 mM NaCl, 1 mM EGTA, 1.5 mM $MgCl_2$, 1% Triton X-100 and 10% glycerol with protease inhibitors (Complete tablets, Roche), Phosphatase Inhibitors (PhosSTOP, Roche), 10 mM iodoacetimide and 4 mM *N*-ethylmaleimide. DNAse I (0.1 mg/ml) was added and incubated for 30 min on ice before centrifugation and incubation with histidine beads or histidine–CUE domain beads overnight at 4 °C. Samples were washed four times with ice-cold PBS, resuspended in SDS–PAGE loading buffer and resolved by western blotting.

Ubiquitin ligase assays.

Ubiquitin-conjugation assays were performed as previously described[43]. Ligase assays were performed in 50 mM Tris-HCl, pH 7.5, 50 mM sodium chloride and 5 mM ATP. The precise concentrations of the proteins and the reaction conditions used varied over the following ranges: 100 ng E1, 25 ng UBE2D1–3 enzymes (Viva Biosciences), 2.5 μg ubiquitin (Sigma) and ~30 ng of ligase proteins. The mixtures were incubated at 37 °C (BRCA1–BARD1) or 30 °C (BMI1–RING1B) for 30–60 min and then stopped with 3× gel-loading buffer, subjected to electrophoresis and western blotting for Ub (P4D1) and BRCA1 (MS110). For comparison of WT- and R99E BARD1–containing heterodimers with mutant D33R Ub, the WT complexes were incubated for 15 min, and the mutant reactions were incubated for 1 h. In reactions examining nucleosome modification, 0.05 μg nucleosomes (Cambridge Bioscience) was added per reaction, as described above.

Ub-transfer reactions.

E2 (UBE2D1 or UBE2D3) was first charged with Ub in the absence of an E3 and a substrate. To prepare the UBE2D1~Ub thioester, we incubated UBE2D1 and Ub (both 100 μM) with 0.2 μM Ube1 in 50 mM Tris, 150 mM NaCl, 3 mM ATP, 5 mM $MgCl^2$, 0.5 mM TCEP and 0.1% (v/v) NP-40, pH 7.5, at 37 °C for 12 min. To stop E1-mediated loading of E2 with ubiquitin, we depleted ATP by adding apyrase (4.5 U ml^{-1}; New England BioLabs). The E2~Ub thioester (~20 μM) was incubated with BRCA1–BARD1, ~30 ng, and 500 mM lysine at room temperature. Reactions were stopped by addition of nonreducing SDS–PAGE loading buffer. The percentage of E2 modified with ubiquitin was determined by quantification of scans with ImageJ software. Reaction time points were taken from 30 s to up to 20 min, and reaction rates were determined with at least three time points within the linear range of the reaction.

Interrogation of protein structures.

The RING domain of BRCA1 (PDB 1JM7 chain A)[18] was superimposed on the RING domain of the RNF4 RING–UBE2D1(S22R C85K)–Ub complex (PDB 4AP4)[13] with Swiss PDB Viewer. Structural representations and models were generated with PyMOL (http://www.pymol.org/). Similarly, the RING domain of BARD1 (PDB 1JM7 chain B) was superimposed on the RING domains of BMI1–RING1B (PDB 2CKL)[40], RAD18 (PDB 2Y43)[41], TRIM37 (PDB 3LRQ) and RBBP6 (PDB 3ZTG)[42] to identify residues similarly located to BARD1 R99.

Cell lines.

The Flp-In doxycycline-inducible HeLa parent cell line was a kind gift from G. Stewart (University of Birmingham), and Flp-In T-Rex doxycycline-inducible HEK 293 cell lines (Life Technologies) were grown in DMEM (Sigma) and 10% tetracycline-free fetal calf serum (Clontech) supplemented with 1% penicillin/streptomycin. All other cell lines were grown in DMEM supplemented with 10% FCS (Sigma) and 1% penicillin/streptomycin. The pCMV-EGFP and pEF-GFP HeLa cell lines were a kind gift from R. Katz (Fox Chase Cancer Center). The 293T cells, but not the HeLa lines, were authenticated at the source. Mycoplasma testing was performed through Hoechst DNA staining.

BARD1-expressing lines.

pcDNA5/FRT/TO-RFP-Flag-BARD1 (human) was engineered to carry silent mutations to confer siRNA resistance (WT, TGGTTTAGCCCTCGAAGTAAG; siRNA-resistant, TGGTTTtcgCCaCGtAGTAAG) and was synthesized by Genscript for WT and L44R variants. The R99E mutation was later introduced by site-directed mutagenesis and confirmed by sequencing. Stable cell lines containing Tet-inducible RFP-Flag-BARD1 were generated in Flp-In HeLa and HEK 293 cells by cotransfection of the pcDNA5/FRT/TO-RFP-Flag-BARD1 constructs with the recombinase pOG44 (Invitrogen) with FuGene6 (Promega). After 48 h, cells were placed into hygromycin selection medium (400 μg/ml) and grown until colonies formed on plasmid-transfected plates but not controls. For protein expression cells were incubated ±doxycycline (1 μg/ml) for 48 h, and positive clones were selected by screening for Flag expression by western blotting. Expression level in the clonal cell population was confirmed by immunofluorescence for RFP. Flp-In 293 T-REx inducible cells expressing BARD1 derivatives were generated from pcDNA5-RFP-Flag-BARD1, recombined as described above.

BRCA1 expressing lines.

Flag-EGFP-BRCA1 (human) inducible Flp-In HeLa cells expressing WT or BRCA1 mutants were generated by cloning Flag-EGFP-BRCA1 into pcDNA5/FRT/TO, recombination and selection as described for BARD1-expressing lines.

H2A-Ub fusion–expressing lines.

Human HIST1H2AC was cloned in frame with an N-terminal HA tag in pCDNA3.1+ by GenScript. As indicated, individual lysines were mutated to arginines by gene synthesis. Human ubiquitin (*UBA52*) was positioned at the N terminus and/or C terminus of H2A with the addition of N-terminal HA tags. cDNA for ubiquitin was mutated at each of the seven lysine residues to arginine to prevent chain formation. The sequences of all constructs were verified by GenScript. Flp-In HeLa cells expressing H2A mutations and fusions were generated by cloning into pcDNA5/FRT/TO, (H2A WT with HindIII and Xho1, and H2A-Ub with HindIII and BamH1), H2A-BFP was cloned directly into pcDNA5, before recombination and selection as described for BARD1-expressing lines.

Myc-SMARCAD1-expressing lines.

Human *SMARCAD1* cDNA was cloned in frame with an N-terminal myc tag into pCDNA5/FRT/TO by gene synthesis (GenScript). The cDNA was rendered siRNA resistant to the two siRNAs used in this study with the following silent mutations (underlined).
siRNA 1 resistance (amino acid sequence 451-ERDVVIRLMN):
gaa aga gat gta gtt ata agg ctt atg aac
gaa aga gac gtc gtc at t cgc ctg atg aac

siRNA 2 resistance (amino acid sequence 981-SQGTIEESML):
agc caa ggg acg att gaa gaa tcc atg cta a
agc caa ggc aca atc gag gag agc atg cta a

The following mutations were introduced to generate the CUE 1+2 mutant: L168E F169E L195E L196E (CUE1) and F263E A285E L286E (CUE2). The ATPase mutant (K528R) was generated by site-directed mutagenesis and confirmed by sequencing.

Transfections.

siRNA transfections were carried out with Dharmafect1 (Dharmacon) and DNA plasmids with FuGENE 6 (3 µl FuGENE per 1 µg DNA) (Promega), per the manufacturer's guidelines.

DNA-repair reporter assays.

DR3 and EJ5 U20S reporter cell lines were simultaneously cotransfected with siRNA with Dharmafect1 (Dharmacon) and DNA (RFP or RFP-BARD1 and I-*SceI* endonuclease expression constructs) with FuGene6 (Promega). After 16 h, the medium was replaced, and cells were grown for a further 48 h before fixation in 2% PFA. RFP and GFP double-positive cells were scored by FACS analysis with a CyAn flow cytometer and a minimum of 10,000 cells counted. Data were analyzed with Summit 4.3 software. Each individual experiment contained three technical repeats and was normalized to siRNA controls or to WT-complemented cells. Graphs shown are combined data from a minimum of three independent experiments, and error bars show standard error. H2A and H2A-Ub fusion constructs were cotransfected with I-*SceI* and RFP as a surrogate marker for transfection efficiency.

Colony assays.

Cells were plated at 2×10^5 cells/ml in a 24-well plate and treated as required. Cells were then trypsinized, transferred to a six-well plate (volume transferred on the basis of plating density experiments). Plates were incubated for 10–14 d. Colonies were stained with 0.5% crystal violet (BDH Chemicals) in 50% methanol and counted. Each individual experiment contained three technical repeats and was normalized to untreated controls. Graphs shown are combined data from a minimum of three independent experiments, and error bars show standard error.

Exposure to DNA-damaging-agents.

Cells were exposed to irradiation with a Gamma-cell 1000 Elite irradiator (cesium-137 source). Cells were exposed to HU overnight before plating. For all other drugs, cells were exposed for 2 h. Camptothecin, etoposide, 4AN, HU, aphidicolin, and cisplatin were from Sigma. Olaparib was from Selleck chemicals.

Laser microirradiation.

Laser microirradiation experiments were performed on BrdU-presensitized cells (10 μM BrdU, 24 h) as previously described[44], with a Zeiss PALM MicroBeam equipped with a 355-nm UV-A pulsed laser and a 40× objective with laser output at 40%, assisted by the PALMRobo-Software supplied by the manufacturer.

Modified measurement of resection tracks (BrdU).

24 h before fixation, cells were incubated with 10 μM BrdU and then with 10 μM olaparib for the last 16 h of treatment. Cells were trypsinized and resuspended in ice-cold PBS to a concentration of 10×10^5 cells/ml. To lyse the cells, 2 μl of sample was placed on a slide and mixed with 7 μl of spreading buffer (200 mM Tris, pH 7.4, 50 mM EDTA and 0.5% SDS) and

incubated for 2 min. Slides were then placed at a shallow angle to cause the droplet to gradually run down the slide, ensuring constant movement of the droplet. Slides were then fixed in 3:1 MeOH/AcOH for 10 min and then stored at 4 °C.

Slides were washed in PBS and blocking solution (2 g BSA, 200 µl Tween 20 and 200 ml PBS) and then incubated with mouse anti-BrdU primary antibody. Slides were then incubated with AlexaFluor rabbit anti-mouse 488. Images were taken on a Leica DM6000B microscope, and analysis was performed with ImageJ software. Lengths were calculated with a scale bar to convert pixels to micrometers, and the ratio of 3.493 pixels/µm was used to measure BrdU track lengths. 50 fibers per treatment were measured and plotted on a whisker plot with GraphPad Prism.

Immunoprecipitation.

BARD1-Flp-In HEK 293 cells were treated with doxycycline (1 µg/ml) for 48 h and lysed in cold nuclear lysis buffer (10 mM HEPES, pH 7.6, 200 mM sodium chloride, 1.5 mM magnesium chloride, 10% glycerol, 0.2 mM EDTA and 1% Triton X-100). For every 10 ml of nuclear lysis buffer, one Complete protease-inhibitor tablet, one PhosSTOP phosphatase-inhibitor tablet (Roche) and 1 µl DNase were added. Precleared lysate combined with washed Flag–agarose beads (Sigma) was incubated with rotation overnight at 4 °C. After three washes with 1 ml PBS with 0.02% Tween, all wash buffer was removed. Samples were either prepared for SDS–PAGE and western blotting by addition of 2× loading buffer and boiling, or were used for E3 ligase assays.

Nickel precipitations (enrichment of Ub conjugates).

Cells transfected with His_6-myc-Ub were lysed directly in 8 M urea buffer (8 M urea, 0.1 M sodium phosphate, pH 6.3, 0.01 M Tris-HCl, pH 6.3, 10 mM β-mercaptoethanol, 5 mM imidazole and 0.2% Triton X-100), harvested and sonicated. They were then mixed with His-Select beads (Sigma), incubated overnight at 4 °C, washed and eluted in sample loading buffer.

Immunofluorescence.

Cells were plated on 13-mm circular glass coverslips at a density of 5×10^4 cells/ml, treated as required. For RPA, BLM and RAD51 staining, cells were preextracted in CSK buffer (100 mM sodium chloride, 300 mM sucrose, 3 magnesium chloride and 10 mM PIPES, pH 6.8) for 1 min at room temperature. For all other staining, cells were first fixed in 4% PFA and permeabilized with 0.2% Triton X-100 in PBS. After blocking in 10% FCS, cells were incubated with primary antibody for 1 h (unless otherwise stated) and with secondary AlexaFluor antibodies for 1 h.

The DNA was stained with Hoechst at 1:20,000. In some images, the DNA stain has been drawn around (but not shown) to illustrate the location of the nucleus.

EdU staining.

Cells were incubated with the nucleoside analog EdU at 10 μM final concentration for 2 h (RAD51/RPA experiments) or 1 h super-resolution imaging before fixation. Staining was carried out with Click-iT EdU Imaging Kits (Life Technologies) according to the manufacturer's instructions.

Microscopy.

For RPA stains, images of immunofluorescence staining were captured on a Zeiss 510 Meta confocal microscope, with three lasers giving excitation at 647, 555 and 488 nM wavelengths. Images at each wavelength were collected sequentially at a resolution of approximately 1024 × 1024 pixels, with a Plan apochromat 100×/1.4 oil objective. All other immunofluorescence staining was imaged with a Leica DM6000B microscope with an HBO lamp with a 100-W mercury short arc UV-bulb light source and four filter cubes, A4, L5, N3 and Y5, to produce excitations at wavelengths of 360, 488, 555 and 647 nm, respectively. Images were captured at each wavelength sequentially with a Plan apochromat HCX 100×/1.4 oil objective at a resolution of 1,392 × 1,040 pixels.

High-resolution fluorescence microscopy.

Z-stack images were taken on an Olympus DeltaVision IX70 microscope. With softWoRx imaging software, z stacks were taken over 2 μm at 0.1-μm intervals at 100× magnification. The images were then deconvolved with softWoRx deconvolution software. Fluorescence intensity profiles were also generated with softWoRx to analyze 30 foci profiles per experiment.

Statistics.

Statistical analysis was by two-sided Students *t* tests throughout. $*P < 0.05$; $**P < 0.01$; $***P < 0.005$. All center values are given as the mean, and all error bars are standard error of the mean (s.e.m.) unless otherwise described.

43. Boutell, C., Sadis, S. & Everett, R.D. Herpes simplex virus type 1 immediate-early protein ICP0 and is isolated RING finger domain act as ubiquitin E3 ligases *in vitro*. *J. Virol.* **76**, 841–850 (2002).

44. Lukas, C., Falck, J., Bartkova, J., Bartek, J. & Lukas, J. Distinct spatiotemporal dynamics of mammalian checkpoint regulators induced by DNA damage. *Nat. Cell Biol.* **5**, 255–260 (2003).